

Metabolic Fate of ^{18}F -FDG in Mice Bearing Either SCCVII Squamous Cell Carcinoma or C3H Mammary Carcinoma

Katrin Kaarstad, MD¹; Dirk Bender, PhD¹; Lise Bentzen, MD²; Ole Lajord Munk, MSc¹; and Susanne Keiding, DSc^{1,3}

¹PET Center, Aarhus University Hospital, Aarhus, Denmark; ²Department of Experimental Clinical Oncology, Aarhus University Hospital, Aarhus, Denmark; and ³Department of Medicine V, Aarhus University Hospital, Aarhus, Denmark

Tumors often have an increased uptake of glucose and can be detected by PET imaging using ^{18}F -FDG. ^{18}F -FDG is converted to ^{18}F -FDG-6-phosphate (^{18}F -FDG-6-P), and the usual assumption is that ^{18}F -FDG-6-P is not a substrate for subsequent enzymatic reactions and that tumor hot spots reflect trapping of ^{18}F -FDG-6-P. We recently found, however, that in the pig liver, ^{18}F -FDG is metabolized not only to ^{18}F -FDG-6-P but also to the subsequent oxygenation product 2- ^{18}F -fluoro-2-deoxy-6-phospho-D-gluconate (^{18}F -FD-PG1). We therefore wished to characterize the metabolism of ^{18}F -FDG in experimental tumors in mice. **Methods:** ^{18}F -FDG was given intravenously to mice with either SCCVII squamous cell carcinoma or C3H mammary carcinoma grown on the back. ^{18}F -Labeled metabolites were determined by radio-high-performance liquid chromatography in tumor tissue biopsies, in a time course of 180 min (12 mice of each tumor type), and in liver tissue biopsies 80 min after tracer injection (2 mice of each type). **Results:** After the tracer injection, not only ^{18}F -FDG and ^{18}F -FDG-6-P but also ^{18}F -FD-PG1 and 2- ^{18}F -fluoro-2-deoxy-1,6-biphosphate were detected in both tumors, relatively more in SCCVII carcinoma than in C3H carcinoma. Both tumors accumulated radioactivity throughout the 180-min measurement period, 4-fold more in SCCVII carcinoma than in C3H carcinoma. At 80 min, the radioactivity was approximately 6 and 1.2 times higher in the respective tumors than in liver tissue. **Conclusion:** Our results agree with the general finding that most malignant tumor tissues accumulate significantly more ^{18}F -radioactivity than do normal tissues, but our results do not support the concept that this increase is caused solely by accumulation of ^{18}F -FDG-6-P. Furthermore, the rate of ^{18}F -FDG metabolism was higher in SCCVII carcinoma than in C3H carcinoma.

Key Words: tumor glucose metabolism; ^{18}F -FDG PET; SCCVII squamous cell carcinoma; C3H mammary carcinoma

J Nucl Med 2002; 43:940–947

Metabolic processes in intact organisms can be imaged and quantified using PET. Because glucose uptake is often increased in tumor tissue (1,2), tumors can be detected by PET

through use of the glucose analog ^{18}F -FDG as a radioactive tracer (3–5). ^{18}F -FDG is transported across the cell membrane by the same carrier mechanism as that which transports glucose, and ^{18}F -FDG is subsequently phosphorylated in parallel to glucose by hexokinase to ^{18}F -FDG-6-phosphate (^{18}F -FDG-6-P). The usual assumption is that ^{18}F -FDG-6-P is not a substrate for subsequent enzymatic reactions and that intracellular trapping of ^{18}F -FDG-6-P (6–9) is the reason for the radioactivity accumulation in tumor hot spots on PET images.

We recently found, however, that in pig liver, ^{18}F -FDG not only is metabolized to ^{18}F -FDG-6-P but also is significantly metabolized to the subsequent oxygenation products, 2- ^{18}F -fluoro-2-deoxy-6-phospho-D-gluconolactone (^{18}F -FD-PGL) and 2- ^{18}F -fluoro-2-deoxy-6-phospho-D-gluconate (^{18}F -FD-PG1) (10). These metabolites started to appear in liver tissue 45 min after the ^{18}F -FDG injection, and their sum reached a level of 40% of the metabolite contents after 180 min. Dienel et al. (11), in studying rat brain, found that 1- ^{14}C -2-deoxy-D-glucose was converted not only to 1- ^{14}C -2-deoxy-D-glucose-1-phosphate but also to 1- ^{14}C -2-deoxy-D-glucose-1,6-biphosphate. To our knowledge, only 1 study (12) has attempted to characterize and quantify the metabolites of ^{18}F -FDG in tumor tissue in vivo. High-performance liquid chromatography (HPLC) on Rous rat sarcoma found that ^{18}F -FDG was metabolized to ^{18}F -FDG-6-P and to several other ^{18}F -labeled metabolites, identified as ^{18}F -FDG nucleotide derivatives of ^{18}F -FDG. Whether the assumption of trapping of ^{18}F -FDG-6-P in tumor tissue is correct, and whether ^{18}F -FDG metabolism is similar in different tumors, are thus open questions. If the metabolism is not similar, what are the consequences for the interpretation of ^{18}F -FDG PET images, for kinetic modeling of ^{18}F -FDG metabolism, and for tumor detection by ^{18}F -FDG PET in oncology? To answer these questions therefore, we wished to conduct a preclinical study that would characterize and quantify ^{18}F -FDG metabolism in experimental carcinomas grown on mice.

MATERIALS AND METHODS

Animals and Tumors

The Danish Animal Experimentation Inspectorate approved the study procedures. Twelve male C3H/KM mice (age range, 12–16

Received Oct. 15, 2001; revision accepted Mar. 25, 2002.

For correspondence or reprints contact: Susanne Keiding, DSc, PET Center, Aarhus University Hospital, DK 8000 Aarhus, Denmark.
E-mail: susanne@pet.auh.dk

wk; body weight range, 27–41 g) with SCCVII squamous cell carcinoma grown on the back and 12 male CDF1 mice (age range, 12–16 wk; body weight range, 30–40 g) with C3H mammary carcinoma grown on the back were used. Derivation and maintenance was as described previously (13). Average tumor volumes were 790–1,180 mm³ (median, 990 mm³) for SCCVII carcinoma and 600–920 mm³ (median, 760 mm³) for C3H carcinoma. The mice were randomly allocated to the time points of the tumor biopsies.

Radiolabeled Tracer

¹⁸F-FDG was produced at the radiochemistry facility of the PET Center of Aarhus University Hospital (Aarhus, Denmark) as previously described (10). The radiochemical purity was >95%, and the specific radioactivity was approximately 72 GBq/μmol. The main impurities were partly hydrolyzed acetylated ¹⁸F-FDG (≤3%) and ¹⁸F-fluoride (≤1%).

Experimental Setup and Tumor Biopsies

The mice fasted for approximately 4 h. They were restrained in lucid plastic jigs with the tails secured with tape to allow an intravenous line to be inserted into the tail vein. The intravenous line consisted of a butterfly needle (25 gauge) and a polyethylene tube. The volume was approximately 70 μL and adjusted for at the tracer injection by flushing with isotonic saline with heparin. The ¹⁸F-FDG was given intravenously in a volume of only 100 μL to minimize changes in the animals' blood volume and circulation. For the SCCVII carcinoma mice, the ¹⁸F-FDG dose was 3.1–5.9 MBq per animal (median, 4.4 MBq per animal). For the C3H carcinoma mice, the ¹⁸F-FDG dose was 2.0–2.7 MBq per animal (median, 2.4 MBq per animal). The mice were anesthetized with 0.40 mL intravenous mebumal (4.76 mg/mL saline) 10 min before the biopsy samples were taken. Biopsies were performed using the through-cut technique (cutting biopsy needle, 2.1-mm diameter; Worldwide Medical Technologies, Woodbury, CT). From 2 animals (for double determinations) of each tumor type, tumor biopsy samples were taken 5, 20, 45, 80, 110, and 180 min after the ¹⁸F-FDG injection and liver biopsy samples were taken at 80 min. Because of the small size of tumors and livers in mice, 3–4 biopsies, each of 6–8 mg, were taken at each time point from each mouse. The animals were killed by cervical dislocation. The tissue samples were immediately transferred into a precooled (liquid nitrogen) custom-made Teflon (DuPont, Wilmington, DE) container. For homogenization, the container held a tungsten ball and was transferred into a mill (mixer mill MM 200; Retsch GmbH and Co., KG, Haan, Germany), in which it was shaken vigorously for 60 s to disintegrate the frozen tissue samples into subcellular fractions (14). After 10 min at room temperature, the samples were thawed and mixed with 1,000 μL phosphate buffer (0.01 mol/L K₂HPO₄/KH₂PO₄, 1.5 mmol/L K₂-ethylenediaminetetraacetic acid disodium salt dihydrate [EDTA], 0.01 mol/L monothiolglycinol, 10% glycinol [v/v], 0.01 mol/L Na₂MoO₄·2H₂O, pH 7.5) by being shaken in the mill for 60 s. The homogenate was divided into 3 samples: 400 μL homogenate were transferred into a V-shaped plastic vial containing 500 μL acetonitrile for protein precipitation, 100 μL were transferred into a vial used for counting radioactivity in a well scintillation counter (Cobra; Canberra Packard, Zurich, Switzerland), and the rest was transferred into a V-shaped plastic vial and stored at –80°C for 1 d, until the protein concentration was measured using the method of Lowry et al. (15). The sample containing acetonitrile was centrifuged (Micromax centrifuge; IEC International Equipment Company, Needham Heights, MA) for 2

min at 13,000 rpm to precipitate the proteins. The supernatant was transferred into a plastic tube, and acetonitrile was evaporated at 20 mm Hg. Finally, the solution was centrifuged for 30 s at 13,000 rpm, and the supernatant was analyzed by radio-HPLC.

In Vitro Enzymatic Preparation of ¹⁸F-FDG-6-P, ¹⁸F-FD-PGL/¹⁸F-FD-PG-1, and 2-¹⁸F-Fluoro-2-Deoxy-1,6-Biphosphate (¹⁸F-FDG-1,6-P₂)

¹⁸F-FDG-6-P (12). Ten milligrams (250–400 units) hexokinase type IV from bakers' yeast (EC 2.7.1.1; Sigma-Aldrich A/S Denmark, Vallensbaek Strand, Denmark) were dissolved in 1 mL 70 mmol/L NaH₂PO₄ buffer. Two milligrams (3.6 μmol) adenosine triphosphate (Sigma-Aldrich A/S Denmark) and 1 mg (5 μmol) MgCl₂·6H₂O (Sigma-Aldrich A/S Denmark) were added. The pH was adjusted to 7.4 using diluted sodium hydroxide solution. Approximately 100 MBq ¹⁸F-FDG were added, and the solution was stirred at room temperature (20°C). Samples were taken, and phosphorylation was followed and analyzed by radio-HPLC. The formation of ¹⁸F-FDG-6-P was confirmed by coinjection with nonradioactive ¹⁹F-FDG-6-P (Sigma-Aldrich A/S Denmark).

¹⁸F-FD-PGL/¹⁸F-FD-PG-1 (12,16,17). These products were prepared by enzymatic oxidation of ¹⁸F-FDG-6-P. ¹⁸F-FDG-6-P was synthesized, and after completion of phosphorylation, 5 mg (6.5 μmol) β-nicotinamide adenine dinucleotide phosphate (β-NADP) (Sigma-Aldrich A/S Denmark) and 35 units glucose-6-phosphate dehydrogenase (EC 1.1.1.49; Boehringer-Mannheim, Mannheim, Germany) were added. After the pH was readjusted with diluted sodium hydroxide solution to 7.2, the solution was stirred at room temperature (20°C). Samples were taken to follow the enzymatic oxidation and were analyzed by radio-HPLC. Because the procedure has been well described in the literature (12,16,17) and enzymatic processes are highly specific, the product was not further characterized.

¹⁸F-FDG-1,6-P₂ (11,18). This product was synthesized enzymatically by conversion of ¹⁸F-FDG-6-P using phosphoglucomutase in the presence of glucose-1,6-diphosphate. ¹⁸F-FDG-6-P was synthesized, and after completion of phosphorylation, 1.1 mg (2.7 μmol) EDTA (Sigma-Aldrich A/S Denmark), 1.3 mg bovine serum albumin (Sigma-Aldrich A/S Denmark), 1.1 mg (1.5 μmol) α-D-glucose-1,6-diphosphate cyclohexylammonium salt (Sigma-Aldrich A/S Denmark), and 20 units phosphoglucomutase (EC.5.4.2.2; Boehringer-Mannheim) from rabbit muscle were added. The mixture was stirred at room temperature (20°C) after the pH was adjusted to 7.9 with diluted sodium hydroxide solution. Samples were taken to follow the enzymatic phosphorylation and were analyzed by radio-HPLC. Because the procedure has been well described in the literature (11,18) and enzymatic processes are highly specific, the product was not further characterized.

Radio-HPLC

Radio-HPLC analysis of the tumor and liver tissue samples was performed on Perkin-Elmer Denmark A/S equipment (Allerød, Denmark) as described previously (10), the only difference being that the pH of the mobile phase (20 mmol/L potassium phosphate buffer) was 6.6 instead of 6.9 to adjust for the relatively high pH of the phosphate buffer. The chromatograms were analyzed using commercially available radiochromatography software (Winnie 3.2; raytest Isotopenmessgeraete GmbH, Straubenhardt, Germany). Radio-HPLC identification of the HPLC findings was done by analysis of products from in vitro enzymatic reactions (12). For radio-HPLC of the biopsy samples, an isocratic LC pump 250 (Perkin-Elmer Denmark A/S) equipped with a Rheodyne 7125

injector (Perkin-Elmer Denmark A/S) and 1-mL stainless steel injection loop connected in series with a SphereClone 5- μ m strong-anion-exchange (SAX) 250 \times 4.6 mm column (Phenomenex, Torrance, CA), an LC 295 UV/Vis detector (Perkin-Elmer Denmark A/S), and a sodium iodide scintillation detector (GABI; raytest) was used. For biopsy samples, only the radioactivity channel was recorded. Chromatograms were analyzed using the Winnie 3.2 software. The mobile phase was 20 mmol/L potassium phosphate buffer, pH 6.6, and the flow rate was 0.8 mL/min. The pH was lowered from the previously reported 6.9 (10) to 6.6 to adjust for the relatively high pH of the phosphate buffer used for tissue extraction. Solutions from the in vitro phosphorylation experiments were analyzed using a binary LC pump 250 equipped with a Rheodyne 7125 injector and a 100- μ L stainless steel injection loop connected in series with a SphereClone 5- μ m SAX 250 \times 4.6 mm anion exchange column, a series 200 refractive index detector (Perkin-Elmer Denmark A/S), and a sodium iodide scintillation detector of in-house design. Chromatograms were analyzed using commercially available chromatography software (Turbochrom 4.1.2; Perkin-Elmer Denmark A/S). The mobile phase was 20 mmol/L potassium phosphate buffer, pH 7.2, and the flow rate was 0.8 mL/min.

Efficiency of Tissue Sample Preparation and Radio-HPLC

For both tumors and liver tissue samples, 95%–98% of the radioactivity in the tissue samples was found in the tissue extracts. Recovery of the injected radioactivity from the HPLC column was 85%–110%, compared with an aliquot sample of standard. The main source of error was the volume determination for aliquot samples.

RESULTS

In Vitro Phosphorylation

¹⁸F-FDG-6-P. ¹⁸F-FDG showed the known high affinity toward hexokinase and was efficiently phosphorylated under the chosen conditions. Ten minutes after the addition of ¹⁸F-FDG to the hexokinase/adenosine triphosphate/MgCl₂ mixture, >90% of radioactivity was in the form of ¹⁸F-FDG-6-P. Remarkably, phosphorylation was also observed in the absence of MgCl₂, but with a much slower reaction rate (90% ¹⁸F-FDG-6-P 30 min after the addition of ¹⁸F-FDG). Obviously, the normal magnesium content of the used glass vials was enough to catalyze the enzymatic phosphorylation. No other radioactive compounds besides ¹⁸F-FDG and ¹⁸F-FDG-6-P were observed, confirming the specificity toward phosphorylation by hexokinase.

¹⁸F-FD-PGL/¹⁸F-FD-PG-1. Five minutes after the addition of β -NADP and glucose-6-phosphate dehydrogenase, formation of the oxidation product was already observed. Compared with phosphorylation, enzymatic oxidation occurred at a slower reaction rate. After 180 min, 80% of the analyzed radioactivity was in the form of ¹⁸F-FD-PGL/¹⁸F-FD-PG-1. No other radioactive products besides ¹⁸F-FDG, ¹⁸F-FDG-6-P, and ¹⁸F-FD-PGL/¹⁸F-FD-PG-1 were observed, confirming the specificity of the enzymatic reaction. Gluconolactones are unstable with respect to hydrolysis, and ring opening occurs with a half-life of 90 s at pH

values > 6.0 (19,20). Thus, the initially formed ¹⁸F-FD-PGL hydrolyzed under the given pH conditions of the enzymatic oxidation (pH 7.2) and HPLC separation (pH 7.2), and the product detected was ¹⁸F-FD-PG-1.

¹⁸F-FDG-1,6-P₂. As reported previously (10,18), formation of the 1,6-diphosphate was observed only in the presence of α -D-glucose-1,6-diphosphate. In the presence of α -D-glucose-1,6-diphosphate as cofactor, ¹⁸F-FDG-1,6-P₂ formed. Three minutes after the start of the enzymatic reaction, 30% of the analyzed radioactivity was already in the form of ¹⁸F-FDG-1,6-P₂. After 22 min, the diphosphate was the main product (83%). No other radioactive products besides ¹⁸F-FDG, ¹⁸F-FDG-6-P, and ¹⁸F-FDG-1,6-P₂ were observed, confirming the specificity of the enzymatic reaction.

Radio-HPLC

The radio-HPLC method allowed efficient separation of ¹⁸F-FDG, ¹⁸F-FDG-6-P, ¹⁸F-FD-PGL/¹⁸F-FD-PG-1, and ¹⁸F-FDG-1,6-P₂. Because of the findings of ¹⁹F nuclear magnetic resonance experiments, 2-¹⁸F-fluoro-2-deoxy-mannose (FDM) and ¹⁸F-FDG-1-P are possible metabolites. These compounds are present in early stages of the metabolism and are therefore of particular importance. However, separation of these compounds from ¹⁸F-FDG and ¹⁸F-FDG-6-P is not possible under the given HPLC conditions. ¹⁸F-FDM coelutes with ¹⁸F-FDG, as confirmed by coinjection of non-radioactive FDG and FDM (reference compounds were purchased from Sigma-Aldrich A/S Denmark). As a test for the separation of ¹⁸F-FDG-1-P from ¹⁸F-FDG-6-P, a mixture of glucose-1-phosphate and glucose-6-phosphate (reference compounds were purchased from Sigma-Aldrich A/S Denmark) was analyzed under the given conditions. Because separation of glucose-1-phosphate from glucose-6-phosphate was not observed, separation of ¹⁸F-FDG-1-P from ¹⁸F-FDG-6-P is unlikely. Figure 1 shows the radio-HPLC findings for a mixture of ¹⁸F-FDG-6-P, ¹⁸F-FD-PGL/¹⁸F-FD-PG-1, and ¹⁸F-FDG-1,6-P₂ obtained by the enzymatic in vitro reaction described above. ¹⁸F-FD-PGL/¹⁸F-FD-PG-1 and ¹⁸F-FDG-1,6-P₂ were prepared separately from ¹⁸F-FDG-6-P and mixed afterward.

¹⁸F-FDG Purity

The purity of the ¹⁸F-FDG used in both in vitro and in vivo experiments was >95%. The main impurities caused by the applied synthetic process were partly hydrolyzed, acetylated ¹⁸F-FDG (\leq 3%) and ¹⁸F-fluoride (\leq 1%). Not being an anion, partly hydrolyzed and acetylated ¹⁸F-FDG elutes with ¹⁸F-FDG. Furthermore, under the given chromatographic conditions, ¹⁸F-fluoride is not separated from ¹⁸F-FDG. On injection of the used ¹⁸F-FDG, no radioactivity eluted after the ¹⁸F-FDG. Thus, the radioactive fractions eluting after ¹⁸F-FDG and ¹⁸F-FDG-6-P cannot be attributed to impurities arising from the used ¹⁸F-FDG formulation and were therefore endogenous products.

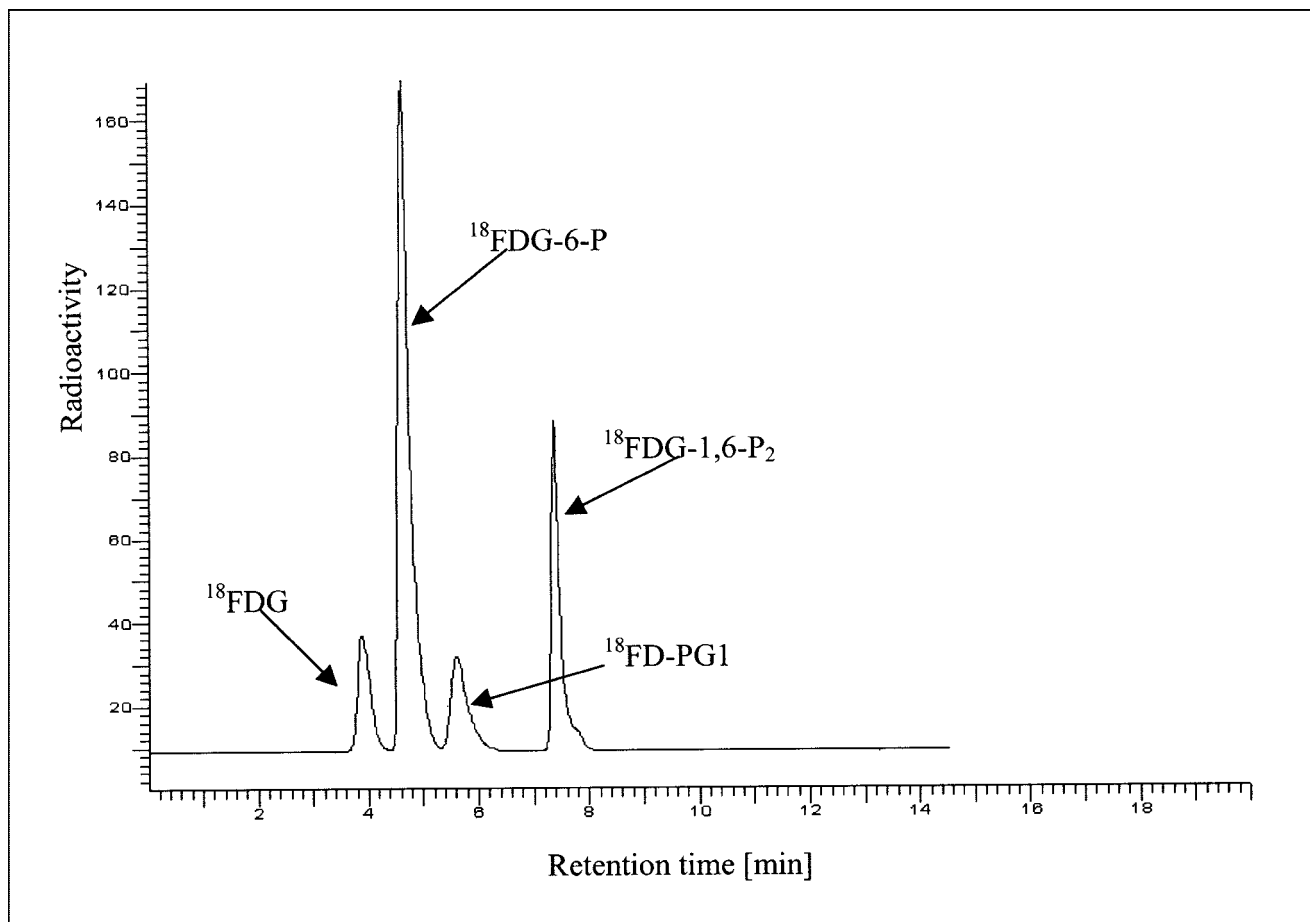


FIGURE 1. Analytic radio-HPLC of mixture of ^{18}F -FDG, ^{18}F -FDG-6-P, ^{18}F -FD-PG1, and ^{18}F -FDG-1,6-P₂. Compounds were prepared individually by *in vitro* enzymatic reactions and mixed afterward (SphereClone [Phenomenex, Torrance, CA] 5- μm SAX 250 \times 4.6 mm column; 20 mmol/L potassium phosphate buffer; pH 7.2; flow rate, 0.8 mL/min).

^{18}F -FDG Metabolites in SCCVII Carcinoma

After the ^{18}F -FDG injection, not only ^{18}F -FDG and ^{18}F -FDG-6-P but also ^{18}F -FD-PG1 and ^{18}F -FDG-1,6-P₂ were detected in the SCCVII carcinoma tissue samples. An example of the HPLC measurements of the tissue extract is shown in Figure 2. Figure 3 shows the time course of the tissue content of ^{18}F -FDG and the 3 metabolites. ^{18}F -FDG decreased rapidly within the first 20 min and then decreased slowly for the rest of the 180-min measurement period. ^{18}F -FDG-6-P appeared early and accounted for half of the radioactivity after 5 min and three fourths after 20 min. Afterward, it remained at that level. ^{18}F -FD-PG1 had already been seen after 5 min and increased steadily until reaching a level of 15% at 180 min. A third metabolite, ^{18}F -FDG-1,6-P₂, appeared after 20 min and increased to 10% after 45 min, followed by a slow decrease throughout the measurement period. The content of other possible metabolites was <0.5% throughout the measurement period. No significant radioactivity was found in the acetonitrile precipitates (which would have contained ^{18}F -labeled glycogen).

^{18}F -FDG Metabolites in C3H Carcinoma

Figure 4 shows the time course of the content of ^{18}F -FDG, ^{18}F -FDG-6-P, and ^{18}F -FD-PG1 + ^{18}F -FDG-1,6-P₂ in C3H carcinoma tissue after the ^{18}F -FDG injection. In Figure 4, the last 2 metabolites are shown as a sum because of their low content in tissue extracts. The time course of ^{18}F -FDG and the metabolites in C3H carcinoma was similar to that in SCCVII carcinoma (Fig. 3), except for the significantly lower content of ^{18}F -FD-PG1 and ^{18}F -FDG-1,6-P₂. The content of other possible metabolites was <0.5% throughout the measurement period. No significant accumulation of radioactivity was found in the acetonitrile precipitates.

^{18}F -FDG Metabolites in Liver

The liver content of ^{18}F -FDG and metabolites at 80 min was similar in mice bearing either carcinoma, being on average 40% for ^{18}F -FDG, 55% for ^{18}F -FDG-6-P, and 7% for ^{18}F -FD-PG1. No ^{18}F -FDG-1,6-P₂ was detectable.

Radioactivity Accumulation in Tumors and Liver

The absolute radioactivity concentrations of ^{18}F -FDG + ^{18}F -metabolites were calculated from the radioactivity concentrations of the tissue homogenates (corrected for radio-

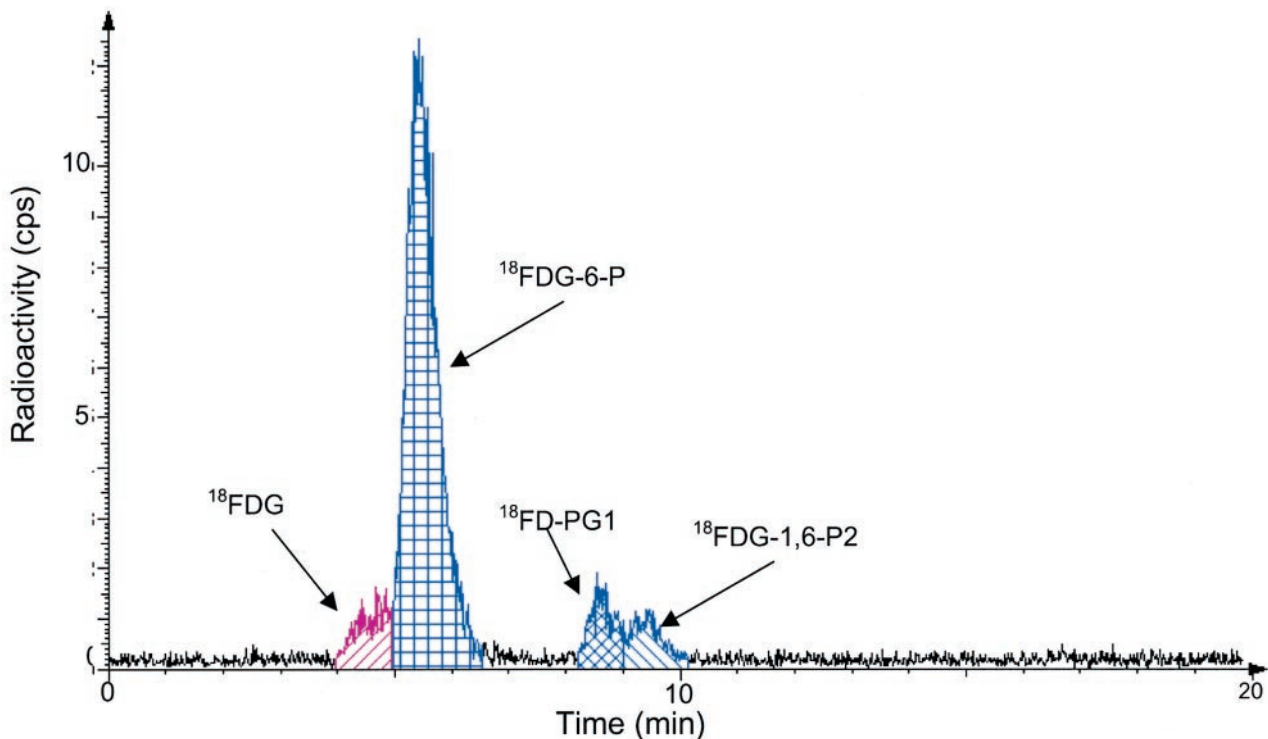


FIGURE 2. Typical radio-HPLC results for analysis of ^{18}F -FDG in squamous tumor tissue extracts 80 min after ^{18}F -FDG injection.

activity decay, with a half-life of 109 min for ^{18}F and the protein concentrations of the homogenates. Figure 5 shows the results normalized for individual ^{18}F -FDG doses. The data were not normalized for body weights or tumor volumes because the ranges of these parameters were narrow.

Both tumor types continued to accumulate radioactivity throughout the 180-min measurement period, and SCCVII carcinoma accumulated 4-fold more radioactivity than did C3H carcinoma (normalized for differences in the tracer doses). At 80 min, the radioactivity was approximately 6

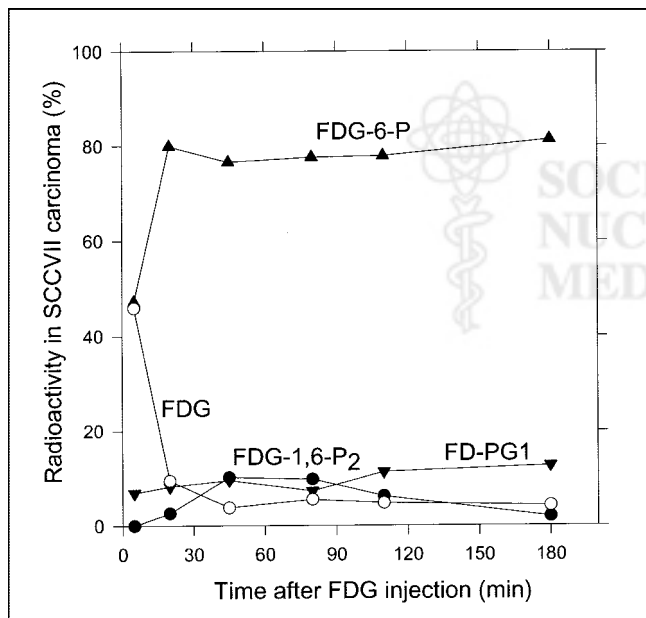


FIGURE 3. Radio-HPLC-determined time course of percentage tissue content of ^{18}F -FDG (○), ^{18}F -FDG-6-P (▲), ^{18}F -FD-PG1 (+ ^{18}F -FD-6-PGL) (▼), and ^{18}F -FDG-1,6- P_2 (●) in SCCVII carcinoma grown on mice.

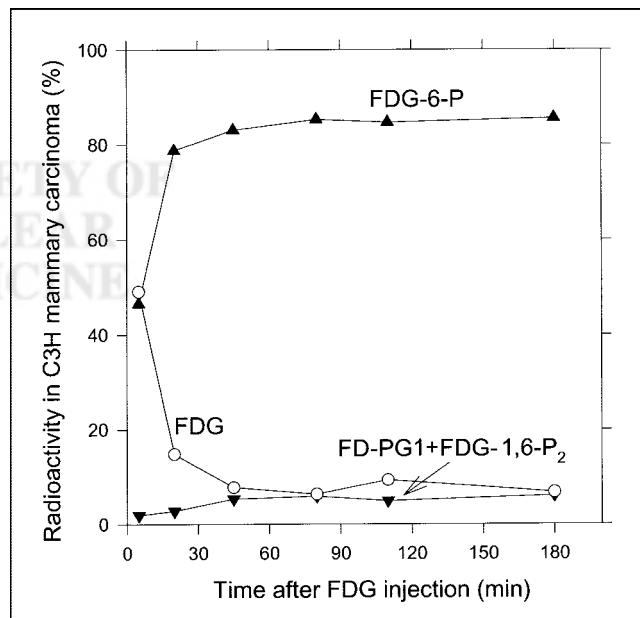


FIGURE 4. Radio-HPLC-determined time course of percentage tissue content of ^{18}F -FDG (○), ^{18}F -FDG-6-P (▲), and ^{18}F -FD-PG1 (+ ^{18}F -FD-6-PGL) + ^{18}F -FDG-1,6- P_2 (▼) in C3H carcinoma grown on mice.

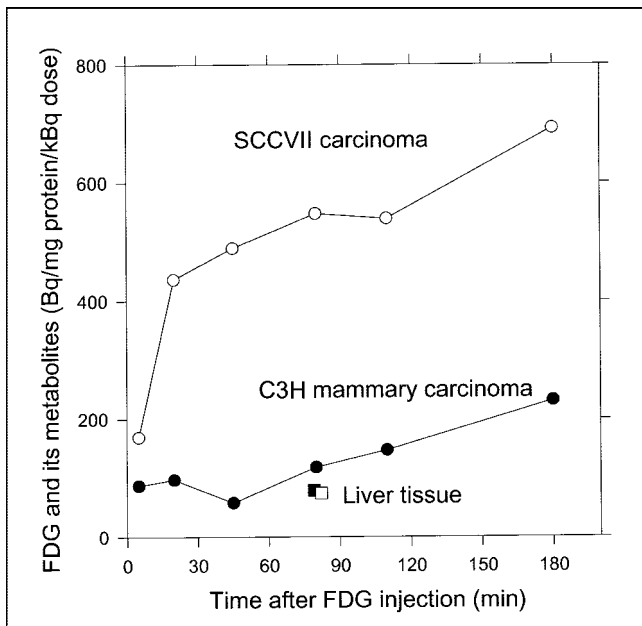


FIGURE 5. Time course of total radioactivity concentrations (^{18}F -FDG + ^{18}F -metabolites) in SCCVII carcinoma (○), C3H carcinoma (●), and liver tissue from respective mice (□, ■). Concentrations are normalized for tissue protein concentrations and individual ^{18}F -FDG doses.

and 1.2 times higher in the respective tumors than in the liver tissue.

DISCUSSION

This study showed, for the first time, the formation of 2 metabolites, ^{18}F -FD-PG1 and ^{18}F -FDG-1,6-P₂, besides ^{18}F -FDG-6-P in malignant tumor tissue in vivo after ^{18}F -FDG administration. All 3 metabolites were found in both SCCVII carcinoma and C3H carcinoma. Figure 6 illustrates the possible metabolic pathways for ^{18}F -FDG-6-P. The findings for ^{18}F -FD-PG1 in the tumors showed that ^{18}F -FDG-6-P was oxidized by tumor glucose-6-phosphate dehydrogenase to ^{18}F -FD-PGL, which was further converted to ^{18}F -FD-PG1 by hydrolysis. The oxidation of ^{18}F -FDG-6-P is reversible (21), whereas the hydrolysis is considered irreversible. As we noted in a previous study on pig liver (10), ^{18}F -FD-6-PGL might be an unstable product and might have been converted to ^{18}F -FD-6-PG1 during tissue sample extraction. The measured ^{18}F -FD-6-PG1 therefore also included ^{18}F -FD-6-PGL. In addition, the presence of ^{18}F -FDG-1,6-P₂ in tumor tissues showed that ^{18}F -FDG-6-P was converted to ^{18}F -FDG-1-P by the phosphoglucomutase. This finding agreed with findings for 1-¹⁴C-2-deoxy-D-glucose (11) and ¹⁹F-FDG in rat brain (22,23). The chromatographic conditions of the HPLC method did not allow for separation of ^{18}F -FDG-6-P from ^{18}F -FDG-1-P, and the figures given for

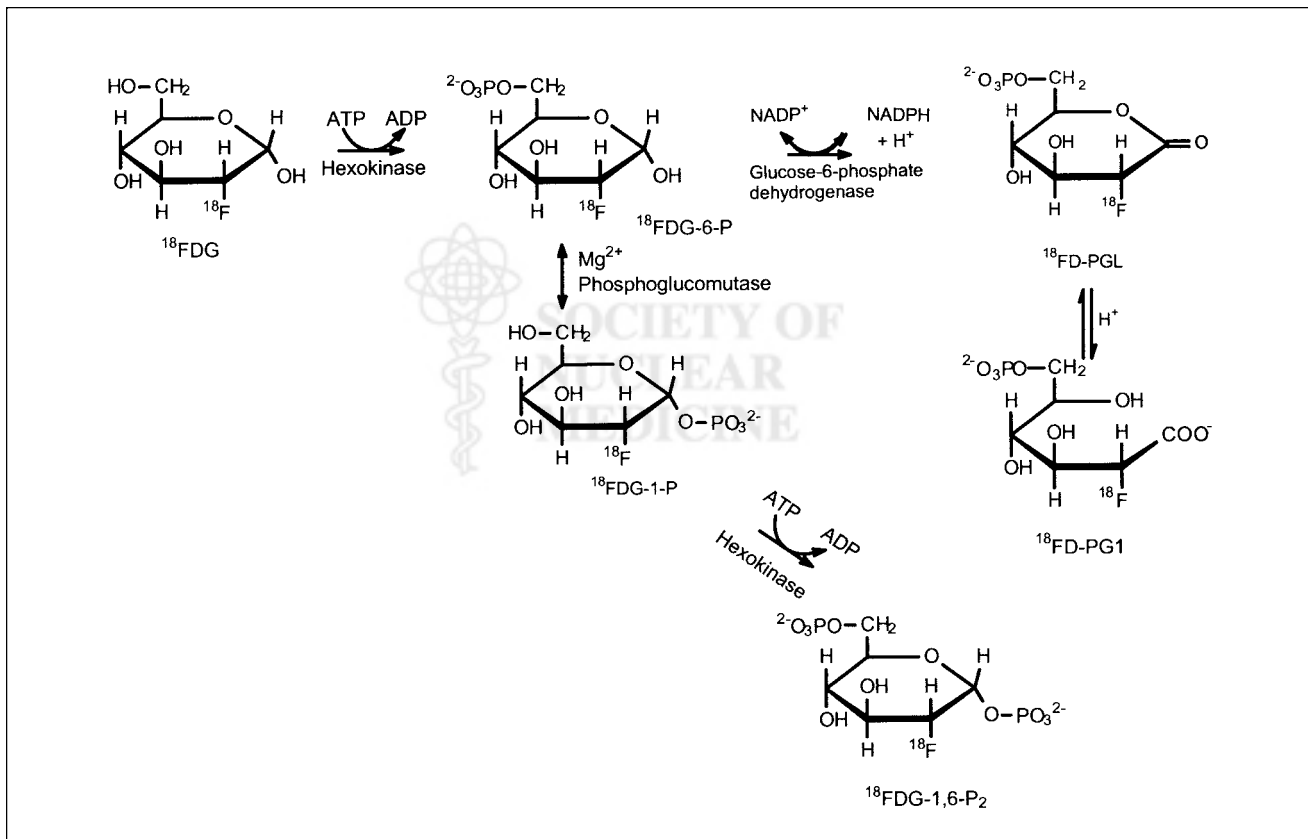


FIGURE 6. Metabolic pathways for ^{18}F -FDG.

^{18}F -FDG-6-P thus might include some ^{18}F -FDG-1-P. Finally, we did not identify any of the nucleotide derivatives of ^{18}F -FDG-1-P or incorporation of ^{18}F -FDG into glycogen, as has been discussed for 1- ^{14}C -2-deoxy-D-glucose (24–27). This finding was in accordance with the results of our previous biopsy experiments on pig liver (10).

The levels of the secondary metabolites, ^{18}F -FD-PG1 and ^{18}F -FDG-1,6-P₂, reached different concentrations in the 2 tumor types, 20% in the SCCVII carcinoma and 8% in the C3H carcinoma (Figs. 3 and 4). In accordance with this finding were the findings of Som et al. (28), that ^{18}F -FDG uptake in tumors depended on both tumor type and animal species, and of Suolinna et al. (12), that only 3% of tumor radioactivity after ^{18}F -FDG injection stemmed from ^{18}F -metabolites other than ^{18}F -FDG-6-P. Accumulation of radioactivity was 4-fold larger in SCCVII carcinoma than in C3H carcinoma (Fig. 5), possibly because of a larger relative number of viable malignant cells in SCCVII carcinoma as judged from the relative content of necrotic tissues (approximately 1% and 30% in SCCVII carcinoma and C3H carcinoma, respectively; M. Horsman, unpublished data, February 2002).

The accumulation of total radioactivity was lower in liver tissue than in either tumor type after 80 min (Fig. 5). Furthermore, the relative amount of ^{18}F -FDG-6-P in liver tissue was low in both mice (50%) and pigs (30% (10)), compared with the high levels seen in tumor tissue (80%, Figs. 3 and 4). In accordance with these findings, Suolinna et al. (12) found that 45 min after ^{18}F -FDG administration, 90% of the ^{18}F -radioactivity in tumor tissue was ^{18}F -FDG-6-P, versus 30% in liver tissue. The low level of ^{18}F -FDG-6-P in liver tissue was probably caused by the reversible transport of ^{18}F -FDG across the liver cell membrane and the degradation of ^{18}F -FDG-6-P in liver tissue (5,29), neither of which occurs in tumor tissue.

The fact that ^{18}F -FDG-metabolites other than ^{18}F -FDG-6-P were found in tumor tissue may have implications for the interpretation of estimated kinetic rate constants in terms of the enzymatic processes as discussed for pig liver (10). However, the current data, with relatively few measurements, do not allow for quantitative evaluations for the rate constants. The finding does not in any way alter the conventional use of ^{18}F -FDG uptake in tumor tissue as an indicator of the rate of glucose use, because the trapped label in tissue still reflects the ^{18}F -FDG phosphorylation rate regardless of whether the label is associated with ^{18}F -FDG-6-P or with the products of ^{18}F -FDG-6-P. It would have been a completely different story if the newly discovered metabolites were products of ^{18}F -FDG directly, that is, in parallel or in competition with the phosphorylation reaction.

CONCLUSION

Our results agree with the general finding that most malignant tumor tissues accumulate significantly more ^{18}F -radioactivity than do normal tissues, but our results do not

support the concept that this increase is caused solely by accumulation of ^{18}F -FDG-6-P. These findings raise the question of whether differences in radioactivity accumulation in human tumors after ^{18}F -FDG injection could be caused by differences in ^{18}F -FDG metabolism. It would be interesting to study these phenomena in different human tumors in vivo.

ACKNOWLEDGMENTS

This study was supported by grants from the Danish Cancer Society and the Danish Research Agency (Freja Program).

REFERENCES

1. Warburg O. *The Metabolism of Tumours*. New York, NY: Richard R. Smith; 1931:129–169.
2. Dang CV, Semenza GL. Oncogenic alternations of metabolism. *Trends Biochem Sci*. 1999;24:68–72.
3. Okazumi S, Isonon K, Enomoto K, et al. Evaluation of liver tumors using fluorine-18-fluorodeoxyglucose PET: characterization of tumor assessment of the effect of treatment. *J Nucl Med*. 1992;33:333–339.
4. Avril N, Menzel M, Dose J, et al. Glucose metabolism of breast cancer assessed by ^{18}F -FDG PET: histologic and immunohistochemical tissue analysis. *J Nucl Med*. 2001;42:9–16.
5. Keiding S, Hansen SB, Rasmussen HH, et al. Detection of cholangiocarcinoma in primary sclerosing cholangitis by positron emission tomography. *Hepatology*. 1998;28:700–706.
6. Phelps ME, Huang SC, Hoffman EJ, Selin C, Sokoloff L, Kuhl DE. Tomographic measurement of local cerebral glucose metabolic rate in humans with (F-18)2-fluoro-2-deoxy-D-glucose: validation of method. *Ann Neurol*. 1979;6:371–388.
7. Gallagher BM, Fowler JS, Gutterman NI, MacGregor RR, Wan CN, Wolf AP. Metabolic trapping as a principle of radiopharmaceutical design: some factors responsible for the biodistribution of [^{18}F]2-deoxy-2-fluoro-D-glucose. *J Nucl Med*. 1978;19:1154–1161.
8. Horton RW, Meldrum BS, Bachelard HS. Enzymatic and cerebral metabolic effects of 2-deoxy-D-glucose. *J Neurochem*. 1985;44:567–573.
9. Wolfgang WA, Schwaiger M, Avril N. Quantitative assessment of tumor metabolism using FDG-PET imaging. *Nucl Med Biol*. 2000;27:683–687.
10. Bender D, Munk OL, Feng H, Keiding S. Metabolites of ^{18}F -FDG and 3-O- ^{11}C -methylglucose in pig liver. *J Nucl Med*. 2001;42:1673–1678.
11. Dienel GA, Cruz NF, Sokoloff L. Metabolites of 2-deoxy- ^{14}C glucose in plasma and brain: influence on rate of glucose utilization determined with deoxyglucose method in rat brain. *J Cereb Blood Flow Metab*. 1993;13:315–327.
12. Suolinna EM, Haaparanta M, Paul R, Härkönen P, Solin O, Sipilä H. Metabolism of 2- ^{18}F fluoro-2-deoxyglucose in tumor bearing rats: chromatographic and enzymatic studies. *Int J Rad Appl Instrum B*. 1986;13:577–581.
13. Overgaard J. Simultaneous and sequential hyperthermia and radiation treatment of an experimental tumor and its surrounding normal tissue in vivo. *Int J Radiat Oncol Biol Phys*. 1980;6:1507–1517.
14. Hansen LL, Andersen J, Overgaard J, Kruse TA. Molecular genetic analysis of easily accessible breast tumour DNA, purified from tissue left over from hormone receptor measurement. *APMIS*. 1998;106:371–377.
15. Lowry OH, Rosebrough NJ, Farr AL, Randall RJ. Protein measurement with the Folin-Phenol reagents. *J Biol Chem*. 1951;193:265–275.
16. Nakada T, Kwee IL, Rao GA, Conboy CB. 19-Fluorine nuclear magnetic resonance spectra of 2-fluoro-2-deoxy-D-glucose and its metabolites. *Biochem Arch*. 1985;1:163–166.
17. Pouremad R, Wyrwicz AM. Cerebral metabolism of fluorodeoxyglucose measured with ^{19}F NMR spectroscopy. *NMR Biomed*. 1991;4:161–166.
18. Kanazawa Y, Yamane H, Shinohara S, et al. 2-Deoxy-2-fluoro-D-glucose as a functional probe for NMR: the unique metabolism beyond its 6-phosphate. *J Neurochem*. 1996;66:2113–2120.
19. Horecker BL, Smyrniotis PZ. Reversibility of glucose-6-phosphate oxidation. *Biochim Biophys Acta*. 1953;12:98–102.
20. Roberts BD, Bailey GD, Buess CM, Carper WR. Purification and characterization of hepatic porcine gluconolactonase. *Biochem Biophys Res Commun*. 1978;84:322–327.
21. Strecker HJ, Korke S. Reversible oxidation of glucose by glucose dehydrogenase. *Nature*. 1951;168:913–914.

22. Kanazawa Y, Momozono Y, Ishikawa M, et al. Metabolic pathway of 2-deoxy-2-fluoro-D-glucose studied by F-19 NMR. *Life Sci.* 1986;39:737–742.
23. Shinohara S, Kanazawa Y, Kojima M. Evaluation of energy metabolism in brain using epimerization of 2-deoxy-2-fluoro-D-glucose by ¹⁹F NMR: the effects of anesthesia. *Magn Res Med.* 1991;21:191–196.
24. Colwell DR, Higgins JA, Denyer GS. Incorporation of 2-deoxy-D-glucose into glycogen: implications for measurement of tissue-specific glucose uptake and utilization. *Int J Biochem Cell Biol.* 1996;28:115–121.
25. Kai Kai MA, Pentreath VW. High resolution analysis of [³H]2-deoxyglucose incorporation into neurons and glial cells in invertebrate ganglia: histological processing of nervous tissue for selective marking of glycogen. *J Neurocytol.* 1980;10:693–708.
26. Doenst T, Taegtmeier H. Complexities underlying the quantitative determination of myocardial glucose uptake with 2-deoxyglucose. *J Mol Cell Cardiol.* 1998;30:1595–1604.
27. Virkamäki A, Risanen E, Hämäläinen S, Utrianen T, Yki-Jävinen H. Incorporation of [3-³H]glucose and 2-[1-¹⁴C]deoxyglucose into glycogen in heart and skeletal muscle in vivo. *Diabetes.* 1997;46:1106–1110.
28. Som P, Atkins HL, Bandyopadhyay D, et al. A fluorinated glucose analog, 2-fluoro-2-deoxy-D-glucose (F-18): nontoxic tracer for rapid tumor detection. *J Nucl Med.* 1980;21:670–675.
29. Munk OL, Bass L, Roelsgaard K, Bender D, Hansen SB, Keiding S. Liver kinetics of glucose analogs measured in pigs by PET: importance of dual-input blood sampling. *J Nucl Med.* 2001;42:795–801.

